not appear to be active, either by itself or in combination with this mode. The size of $\lambda_1^{(6)}$ reflects the narrow width of the mixed-valence band. The small value can be explained by cancellation effects in contributions to the b_{2g}* and b_{3u} OVC that contribute to $\lambda_1^{(6)}$—see the discussion preceding eq 11. The data of Krausz and Ludi[19] strongly suggest that the origin of the high-energy tail of the mixed-valence band (and of the weak shoulder, if present) arises from non totally symmetric vibronic interactions not included in our model.

The parameter λ^{PKS} is a measure of the extent of vibronic coupling to $Q_2 = Q_-$, the active mode in the PKS model.[3] Following Wong and Schatz, we estimate λ^{PKS} from the difference in bond lengths between the oxidized and reduced forms of the metal ion centers to be 1.1.[11] For the C-T ion when λ^{PKS} has this magnitude, vibronic coupling to Q_2 has very little effect on the band shape.

While electronic parameters have a large effect on band positions and g values, they have no effect on the band shape of individual bands. However, vibronic parameters *do* have a noticeable effect on the g values—particularly on g_x. The effect is, however, small for changes in these parameters of the magnitude of those illustrated in Figures 5-7.

Our analysis in this paper is directed specifically at the C-T ion. However, the methods used are presented in a general form and can be easily applied to other ions.

Acknowledgment. This work was supported under National Science Foundation Grants CHE8604470 and R11-8600354 and in part under Grant CHE8400423. Most of the calculations were made possible by a grant of time by the Pittsburgh Supercomputing Center. I also acknowledge many useful discussions with Professor Paul N. Schatz and the able assistance of Kelly Lenz and Suzanne Szak with the computer programming and of Wei Tang with the figures. Thanks also go to the University of Virginia for its hospitality during my year there under the NSF/VPW program.

Electric Field Induced Intramolecular Electron Transfer in Spiro π-Electron Systems and Their Suitability as Molecular Electronic Devices. A Theoretical Study

Abbas Farazdel, Michel Dupuis,* Enrico Clementi, and Ari Aviram[†]

Contribution from IBM Corporation, Data Systems Division, Department 48B/MS 428, Kingston, New York 12401. *Received October 30, 1989*

Abstract: Intramolecular electron-transfer properties and their dependence on an external electric field are studied for a typical rigid spiro $\pi-\sigma-\pi$ molecular cation by ab initio MO methods. Our study indicates that the molecule exhibits characteristics appropriate for molecular device applications. Formulas and algorithms are presented for the calculation of the ubiquitous electron-transfer matrix element.

The direction of research in modern electronic technology is leading toward the development and fabrication of ever more miniature electronic components. At the same time, there have been significant advances on both theoretical[1-3] and experimental[2] fronts supporting the idea that it may be possible to develop devices of the size of individual molecules, i.e., molecular electronic devices. A class of molecules originally proposed by Aviram and Ratner[1] and later expounded by Aviram[3] as strong candidates for molecular electronic devices is of the $\pi-\sigma-\pi$ type. These molecules consist of a conductor (C) and a proconductor (PC)[4] π-electron moiety separated by a rigid σ bridge. In order for such a molecule to function as a device, the C site should effectively be insulated from the PC site[3] (see below). This is achieved by having a spirocycloalkane as the σ bridge, making the plane of the C unit perpendicular to that of the PC unit. A group of molecules that meet these requirements is exemplified by the molecular cation **1**:

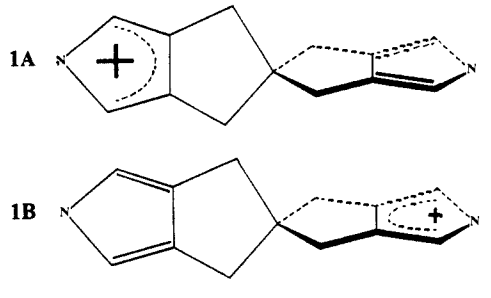

Here **1A** and **1B** represent two possible localized electronic structures of **1**. We refer to **1A** as a left-localized or an A state and to **1B** as a right-localized or a B state.

Qualitatively, **1** and other molecules of this type can be looked upon as a double-well potential for an electron that can hop back and forth between the two wells at some characteristic frequency, which depends on the height and the shape of the potential barrier.[5] Such a two-state molecule conceivably can serve as a binary system in which one state represents "on" and the other represents "off". In this case the two minima should be separated by a sufficiently high barrier corresponding to a small characteristic frequency, so that neither tunneling nor thermal fluctuations can unintentionally switch one state to the other. Only by an external control

[†]IBM Thomas J. Watson Research Center, Yorktown Heights, NY 10598.

(1) Aviram, A.; Ratner, M. A. *Chem. Phys. Lett.* **1974**, *29*, 277; *Bull. Am. Phys. Soc.* **1974**, *19*, 341. Aviram, A. IBM Research Report RC 9953 (No. 43939) March 28, 1983.

(2) Carter, F. L., Ed. *Molecular Electronic Devices*; Marcel Dekker, Inc.: New York, 1982; *Molecular* Electric Devices *II*; Marcel Dekker, Inc.: New York, 1987. Third International Symposium on Molecular Electronic Devices, Washington DC, October 1986; Roland Etvos Physical Society, Satellite Symposium on Molecular Electronics, Budapest, Hungary, August 1987.

(3) Aviram, A. *J. Am. Chem. Soc.* **1988**, *110*, 5687.

(4) The "conductor" (C) form of a compound has a partially filled highest occupied molecular orbital (HOMO) and therefore a partially filled conduction band in the solid state. On the other hand, the proconductor form of the same compound has a fully occupied HOMO and is nonconductive. The C and PC forms are related to each other by either oxidation or reduction as the case may be. For more details, see: Reference 3, and further references therein.

(5) Merzbacher, E. *Quantum Mechanics*; 2nd ed.; John Wiley & Sons: New York, 1970. Eliasson, B.; Staley, S. W. *Prepr.—Am. Chem. Soc., Div. Pet. Chem.* **1985**, *30*, 620.

0002-7863/90/1512-4206$02.50/0

(in this report we use a uniform electric field) should one be able to switch. The height and other attributes of the barrier, and hence the characteristic frequency, can be fine tuned by chemical modifications and structural engineering. For instance, in order to have a high barrier, the plane of the C unit in **1** was chosen to be perpendicular to that of the PC unit so that the two π systems would have the least overlap.

The main function of **1** as a molecular memory device is its intramolecular electron-transfer (ET) capability, which can be represented by the charge-shift reaction **1A** → **1B**. In order to read off the stored information from such a memory device, one can probe the two π terminals of **1** for conductivity, since by electron transfer the PC site becomes conductive while the C site becomes insulating. In turn, inducing electron transfer can be achieved by applying an electric field[3] directed along the axis that connects the spiro carbon of **1** to the terminal nitrogen atoms. Hence, a major objective of this article is to address some of the questions regarding intramolecular ET characteristics of **1** and their electric field dependencies by using LCAO–MO SCF ab initio electronic structure techniques. Specifically, we examine the effect of a uniform external electric field in the range of 0.0–0.005 au (1 au of electric field strength equals 5.1423×10^9 V/cm) on appropriate potential energy surfaces, energetics (intramolecular reorganization energy, exothermicity, and activation energy), and the ubiquitous many-electron electron-transfer matrix element V_{AB}.

Our results show that while exothermicity increases linearly with the electric field strength, intramolecular reorganization energy remains effectively unchanged and activation energy (both diabatic and adiabatic) decreases. The latter corresponds to an increase in ET rate. This and other related behaviors are rationalized by using a simple model based on the traditional theory of a molecule in a weak electric field[6] and the fact that changes in the geometry of **1** during the ET reaction is small. We find V_{AB} to be not significantly sensitive with respect to variations in electric field strength or nuclear configuration in the range of interest. The latter indicates that Condon approximation[7] is valid for molecule **1**. The numerical evaluation of V_{AB}, indcluding a suggested algorithm and derivation of relevant expressions, is detailed in the Appendix. These expressions are in terms of standard LCAO–MO eigenvectors and ready for coding.[8] We introduce a "generalized" density matrix, which simplifies the expressions and their numerical computations.

An Overview of Intramolecular Electron-Transfer Models

It is not necessary here to delve deeply into the theory of ET. Only a brief introduction of some general concepts and definitions follow. Particular attention is given to the significance of the electron-transfer matrix element V_{AB} in different theories of intramolecular ET. For greater detail and more specific references, the reader is referred to the large body of literature on ET, for example, excellent reviews by Dogonadze et al.,[9] Sutin,[10] Newton and Sutin,[11] and Mikkelsen and Ratner,[12] as well as monographs by Ulstrup,[7] Cannon,[13] and DeVault.[14]

Marcus' Model. In ET reactions the transfer of electron is accompanied by nuclear rearrangements. Therefore, it is convenient to consider the potential energy of the system (here molecule **1**)[15] as a function of nuclear coordinates Q, i.e., potential energy surface (PES). The PES of the initial state (**1A**) with left-localized electronic state Ψ_A has a global minimum that corresponds to its equilibrium nuclear configuration Q_A. Similarly, the final state (**1B**) has its own PES and global minimum Q_B with right-localized electronic state Ψ_B. Clearly $Q_A \neq Q_B$ since after transfer of electron the nuclei involved will "see" a different electronic potential and consequently will have a different equilibrium configuration. A cross section of two typical PESs is sketched in Figure 1. The two minima differ in energy by an amount $|\Delta E|$ defined as exothermicity.

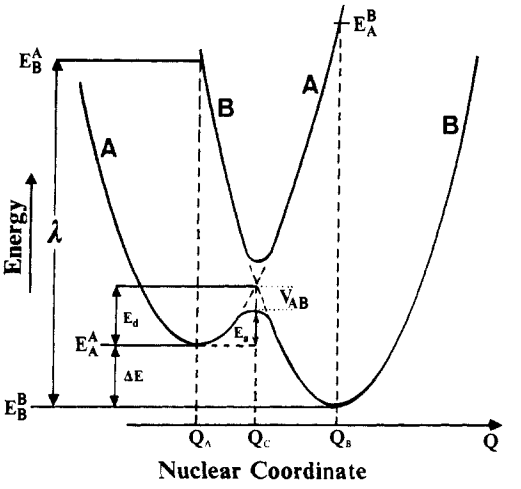

Figure 1. A cross section of an energy profile for initial state A and final state B in a typical electron-transfer reaction. The solid curves are the adiabatic surfaces, but the dashed lines refer to diabatic surfaces. Q_A and Q_B are equilibrium nuclear coordinates of A state and B state, respectively, and Q_C is the nuclear coordinate corresponding to the lowest energy on the crossing seam surface. Intramolecular reorganization energy λ, exothermicity $|\Delta E|$, diabatic activation energy E_d, adiabatic activation energy E_a, and electron-transfer matrix V_{AB} are indicated.

An important quantity in any ET theory is the "interaction energy"; also referred to as "electronic coupling matrix element", $H_{AB} = \langle \Psi_A | H | \Psi_B \rangle$, where H is the total electronic Hamiltonian (excluding nuclear kinetic energy and nuclear repulsion terms) of the system. Usually H_{AB} is very weak (about a few kilojoules per mole) in ET reactions. If it is assumed that there is no interaction at all between **1A** and **1B**, i.e., $H_{AB} = 0$, the two (here called zero-order or diabatic) PESs intersect on a crossing seam, where **1A** and **1B** have the same energy and nuclear configuration Q_C (see Figure 1). In this perspective, ET is a transition from the diabatic surface A to the diabatic surface B (see Figure 1)[16] and is governed by the Franck–Condon principle.[17] This principle requires the nuclear configuration to remain the same during the transition. The only way to meet this requirement in addition to the "conservation of energy", is for ET to occur at the seam of the crossing.

Conversely, if $H_{AB} \neq 0$, i.e., the diabatic states Ψ_A and Ψ_B do not diagonalize the electronic Hamiltonian H, the degeneracy at the crossing of the diabatic surfaces will be effectively removed (the well-known avoided crossing) and two new and separate (now called first-order or adiabatic) PESs are formed (Figure 1). The splitting between the two surfaces can be obtained (within the framework of the two-state model; see below) by solving the secular equation

$$\begin{vmatrix} H_{AA} - E & H_{AB} - ES_{AB} \\ H_{AB} - ES_{AB} & H_{BB} - E \end{vmatrix} = 0 \qquad (1)$$

(6) Buckingham, A. D. *Adv. Chem. Phys.* **1967**, *12*, 107.
(7) Ulstrup, J. *Charge Transfer Processes in Condensed Media*; Springer-Verlag: New York, 1979.
(8) We are not aware of any author who has published these expressions, although several have reported numerical values for V_{AB}. For example, see: Logan, J.; Newton, M. D. *J. Chem. Phys.* **1983**, *78*, 4086. Cave, R. J.; Baxter, D. V.; Goddard, W. A., III; Baldeschwieler, J. D. *J. Chem. Phys.* **1987**, *2*, 926. Reference 27. Reference 31.
(9) Dogonadze, R. R.; Kuznetsov, A. M.; Maragishvili, T. A. *Electrochim. Acta* **1980**, *25*, 1.
(10) Sutin, N. *Prog. Inorg. Chem.* **1983**, *30*, 441.
(11) Newton, M. D.; Sutin, N. *Annu. Rev. Phys. Chem.* **1984**, *35*, 437.
(12) Mikkelsen, K. V.; Ratner, M. A. *Chem. Rev.* **1987**, *87*, 113.
(13) Cannon, R. D. *Electron Trans Reactions*; Butterworth: Stoneham, MA, 1980.
(14) DeVault, D. *Quantum-Mechanical Tunneling in Biological Systems*; Cambridge University Press: Cambridge, U.K., 1984.
(15) Obviously, we are neglecting solvent and counterion effects. Our system consists of only molecule **1** in gas phase.
(16) Strictly speaking, there will not be any electron transfer for diabatic surfaces since diabaticity requires the electrons to remain localized on individual molecules.
(17) Franck, J. *Trans. Faraday Soc.* **1925**, *21*, 536. Condon, E. U. *Phys. Rev.* **1928**, *32*, 858.

where $S_{AB} = \langle\Psi_A|\Psi_B\rangle$, $H_{AA} = \langle\Psi_A|H|\Psi_A\rangle$, $H_{BB} = \langle\Psi_B|H|\Psi_B\rangle$, and E is the energy eigenvalue. Hence the separation Δ between the adiabatic surfaces E_+ and E_- is

$$\Delta(Q) = E_+ - E_- = 2(1 - S_{AB}^2)^{-1}|{}^1/_4(H_{AA} - H_{BB})^2 - (H_{AA} + H_{BB})H_{AB}S_{AB} + H_{AA}H_{BB}S_{AB}^2 + H_{AB}^2\}^{1/2}$$

where E_+ is the higher and E_- is the lower root of eq 1. Conventionally, half of the separation evaluated at the seam of the crossing Q_C where $H_{AA} = H_{BB}$, is designated by V_{AB} (Figure 1). With the latter simplification one obtains

$$V_{AB} = {}^1/_2\Delta(Q = Q_C) = (1 - S_{AB}^2)^{-1}|H_{AB} - S_{AB}(H_{AA} + H_{BB})/2| \quad (2)$$

Note that eq 2 is written in a form that reflects the essential symmetry with respect to the arbitrary labels A and B. The separation parameter V_{AB} is usually referred to as an electron-transfer matrix element. As the name implies, V_{AB} is a key quantity in ET models and in fact it appears, one way or another, in classical,[18] semiclassical,[19] and quantum mechanical[20,21] treatment of ET (see below). V_{AB} can also be interpreted as a measure of the strength of the coupling (or mixing) between the initial state A and the final state B. Note that only in the limit of small S_{AB}, $V_{AB} \simeq H_{AB}$.

The above considerations constitute the essence of the classical Marcus' theory[18] for the so-called adiabatic ET. In this model V_{AB} is assumed to be large enough ($V_{AB} \gg k_BT$) so that the system remains an eigenstate of the true Hamiltonian (i.e., stays on the lower adiabatic curve) at all times during ET and the upper curve may be neglected. As is often done, the so-called two-state model is adopted here; i.e., it is assumed that only two electronic states, here A and B, need be considered and coupling with other electronic states is disregarded. For Marcus' model, the rate constant in Eyring's transition-state theory[22] can be written as[23]

$$k_{TST} = \kappa(k_BT/h)\exp(-\Delta G^*/k_BT) = \kappa(k_BT/h)\exp(\Delta S^*/k_B)\exp(-\Delta H^*/k_BT) \quad (3)$$

where κ is the electronic transmission coefficient (see below), k_BT/h the effective vibrational frequency associated with the activating motion,[24] k_B the Boltzmann constant, and h Planck's constant; ΔG^*, ΔS^*, and ΔH^* are the activation free energy, entropy, and enthalpy, respectively, for the thermal electron-transfer reaction. Equation 3 can be related to the Arrhenius equation

$$k = A\exp(-E_{act}/k_BT) \quad (4)$$

if the preexponential factor A is identified with $\kappa(k_BT/h)\exp(\Delta S^*/k_B)$ and activation energy E_{act} with ΔH^*.[25]

The transmission coefficient κ in eq 3 can be thought of as a Landau–Zener[26] type transition probability, i.e., the probability that the system will make a transition from A surface to B surface on passing through the seam of the crossing. The introduction of κ enables us to treat even nonadiabatic ET reactions within the framework of Marcus' model and provides a link to the quantum mechanical treatment. For adiabatic ET, κ is unity for systems that have enough thermal energy E to overcome the barrier. On the other hand, for nonadiabatic ET, $\kappa \ll 1$ and V_{AB} is so small ($V_{AB} \ll k_BT$) that the time spent by the system at the crossing seam is too short for the wave function to evolve from A state to B state. In this case, the system passes the crossing seam on the A surface and lapses back many times, depending upon the value of κ, which in turn depends on V_{AB}, thermal energy E, and slopes of the diabatic surfaces A and B at the crossing seam,[26] before making a transition to the B surface.

Quantum Mechanical Model. It is possible and perhaps more proper to view a nonadiabatic electron-transfer reaction of an extended system as the nonradiative decay of an initial set of vibronic states $\{|A\upsilon\rangle\}$

$$|A\upsilon\rangle = \Psi_A(q; Q)X_{A\upsilon}(Q) \quad (5)$$

into a dense continuum manifold of vibronic states $\{|Bw\rangle\}$

$$|Bw\rangle = \Psi_B(q; Q)X_{Bw}(Q) \quad (6)$$

where q denotes the electronic coordinates and Q the nuclear coordinates; Ψ_A and Ψ_B are Born–Oppenheimer electronic states characterized by vibrational wave functions $X_{A\upsilon}$ and X_{Bw}, respectively.

Based on Fermi's golden rule of the first-order time-dependent perturbation theory,[20,21] the transition probability $W_{A\upsilon}$ for the reaction $|A\upsilon\rangle \rightarrow \{|Bw\rangle\}$ is given by

$$W_{A\upsilon} = \frac{2\pi}{\hbar}\sum_w|\langle A\upsilon|H'|Bw\rangle|^2\delta(\epsilon^\circ_{A\upsilon} - \epsilon^\circ_{Bw}) = \frac{2\pi}{\hbar}\sum_w|\langle X_{A\upsilon}|H'_{AB}|X_{Bw}\rangle|^2\delta(\epsilon^\circ_{A\upsilon} - \epsilon^\circ_{Bw}) \quad (7)$$

after using eqs 5 and 6. Here H' is the perturbation that causes the electron transfer, $H'_{AB} = H'_{AB}(Q) = \langle\Psi_A|H'|\Psi_B\rangle$, $\epsilon^\circ_{A\upsilon}$ and ϵ°_{Bw} are the unperturbed energy of the vibronic levels $|A\upsilon\rangle$ and $|Bw\rangle$, respectively, and the Dirac δ function ensures energy conservation. It is common to invoke the Condon approximation,[7] according to which H'_{AB} is assumed to be only weakly dependent on nuclear coordinates Q provided the distance between the C and PC units remains unchanged. Then H'_{AB} is factored out of the sum in eq 7 and is replaced by its value at the crossing seam nuclear configuration Q_C. We will see later that this approximation holds quite well for molecule **1**. In addition, the zero-order electronic states Ψ_A and Ψ_B being broken-symmetry charge-localized solutions, it can be shown[27] that the quantity H'_{AB} at the crossing seam is indeed equal to V_{AB}, the same electron-transfer matrix element given by eq 2. At any rate, now eq 7 can be written as

$$W_{A\upsilon} = \frac{2\pi}{\hbar}|V_{AB}|^2\rho_f(\epsilon^\circ_{A\upsilon}) \quad (8)$$

$$\rho_f(\epsilon^\circ_{A\upsilon}) = \sum_w|\langle X_{A\upsilon}|X_{Bw}\rangle|^2\delta(\epsilon^\circ_{A\upsilon} - \epsilon^\circ_{Bw}) \quad (9)$$

where $\rho_f(\epsilon^\circ_{A\upsilon})$ stands for the density of final states of energy $\epsilon^\circ_{A\upsilon}$ weighted by the Franck–Condon factor $|\langle X_{A\upsilon}|X_{Bw}\rangle|^2$. Again we see the prevalent role that V_{AB} plays also in quantum mechanical description of ET. Finally, the thermally averaged ET probability W_A for the reaction $\{|A\upsilon\rangle\} \rightarrow \{|Bw\rangle\}$ is

$$W_A = \frac{1}{Z}\sum_\upsilon\exp(-\epsilon^\circ_{A\upsilon}/k_BT)W_{A\upsilon}$$

where $Z = \sum_\upsilon\exp(-\epsilon^\circ_{A\upsilon}/k_BT)$ and Boltzmann distribution is assumed over the initial manifold $\{|A\upsilon\rangle\}$.

Results and Discussion

All the results presented here, are based on open-shell spin-unrestricted Hartree–Fock (UHF) broken-symmetry diabatic wave

(18) Marcus, R. A. *J. Chem. Phys.* **1956**, *24*, 966; *Can. J. Chem.* **1959**, *37*, 155; *Discuss. Faraday Soc.* **1960**, *29*, 21. Hush, N. S. *Trans. Faraday Soc.* **1961**, *57*, 155. Marcus, R. A. *J. Annu. Rev. Phys. Chem.* **1964**, *15*, 155; *J. Chem. Phys.* **1965**, *43*, 679; *Electrochim. Acta* **1968**, *13*, 995. Waisman, E.; Worry, G.; Marcus, R. A. *J. Electroanal. Chem.* **1977**, *82*, 9.

(19) Brunschwig, B. S.; Logan, J.; Newton, M. D.; Sutin, N. *J. Am. Chem. Soc.* **1980**, *102*, 5798.

(20) Dolin, S. P.; German, E. D.; Dogonadze, R. R. *J. Chem. Soc., Faraday Trans. 2* **1977**, *73*, 648. Kestner, N. R.; Logan, J.; Jortner, J. *J. Phys. Chem.* **1974**, *78*, 2148.

(21) Newton, M. D. *Int. J. Quantum Chem., Quantum Chem. Symp.* **1980**, *14*, 363.

(22) Eyring, H. *J. Chem. Phys.* **1935**, *3*, 107; *Chem. Rev.* **1935**, *17*, 65.

(23) In this classical model the nuclear tunneling effects are neglected. For a semiclassical model in which a nuclear tunneling factor is introduced, refer to: Reference 19.

(24) We are assuming there is only one vibrational mode contributing to the barrier height ΔG^*, and the energy of this vibration is sufficiently low that we can equate it to its classical value k_BT.

(25) If we define E_{act} from the Arrhenius equation by $E_{act} = -k_B[\mathrm{d}\ \ln k/\mathrm{d}(1/T)]$ and neglect the temperature dependence of ΔS^* and ΔH^*, then the appropriate identifications will be $E_{act} = \Delta H^* + k_BT$ and $A = \kappa e(k_BT/h)\exp(\Delta S^*/k_B)$. This correction to E_{act}, however, is usually neglected since k_BT is normally much smaller than ΔH^*.

(26) Landau, L. D. *Phys. Z. Sowjetunion* **1932**, *1*, 88; **1932**, *2*, 46. Zener, C. *Proc. R. Soc. London, Ser. A* **1932**, *137*, 696; **1933**, *140*, 660.

(27) Ohta, K.; Closs, G. L.; Morokuma, K.; Green, N. J. *J. Am. Chem. Soc.* **1986**, *108*, 1319.

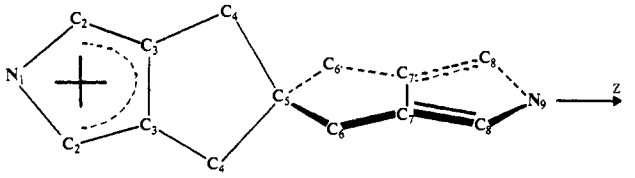

Figure 2. Numbering convention for molecular cation **1** used for Table I. The molecule has C_{2v} symmetry with the shown z axis as its C_2 axis. The plane on the right side of the spiro carbon (C_5) is perpendicular to that of the left side. The molecular frame shown is referred to as the A frame in the text. The charge of the molecule is localized on the left, i.e., it is an A state. If the charge is localized on the right, it would be a B state. The B frame can be obtained from the A frame by appropriate rotations (see the text).

functions using the latest version of the HONDO package of computer codes.[28] For the calculation of off-diagonal elements H_{AB},S_{AB}, and V_{AB}, we have developed a set of program modules that are linked to HONDO. In these modules we use the "corresponding orbital transformation" as expounded by King et al.[29] This approach has also been used by previous workers.[21,30,31] For details see the Appendix, where the needed formulas in terms of standard outputs of molecular programs are developed. In our derivation, we introduce a "generalized" density matrix in terms of which the expressions formally look like one-electron and two-electron contributions to total energy.

Diabatic Equilibrium Structures. The geometry of **1** was completely optimized with C_{2v} symmetry for the framework of the molecule and no external electric field. The initial guess used in the optimization process was the equilibrium structure for the neutral analogue of **1** at the restricted Hartree–Fock (RHF) level for which we defined localized molecular orbitals. The optimization algorithm then yielded the structures A and B. The C_{2v} point group was used here because it is the highest allowed symmetry that still permits electron localization on either C or PC site. During the optimization, we made certain the SCF wave functions were localized on the appropriate side of the spiro carbon in the molecule. This was done by monitoring the electronic population at every stage of the optimization process. In general to induce a left-localized or a right-localized SCF solution, it was usually adequate to start with one as the initial guess. In turn in order to prepare the needed localized initial guess, sometimes we used the Boys' localization method[32] and other times we took a routinely obtainable delocalized solution and replaced two appropriately selected orbitals in it by their sum and difference. Occasionally it was necessary to use the converged localized results of a similar case as the initial guess. We used both STO-3G and 3-21G[33] basis sets in order to make sure the optimized geometry is not too sensitive to the type of basis set used. The maximum difference between the two geometries was 0.018 Å for bond lengths and 0.5° for bond angles. Table I shows the optimized geometry when the spin population (or "unpaired electron") and hence the positive charge is localized on the left side of the nuclear framework of the molecule. We designate this wave function as A state (i.e., charge localized on the left like **1A**), the geometry as A frame (the optimized geometry of **1A** as shown in Figure 2 and Table I), and its total energy as E_A^A. Hereafter, the uppercase subscript of "E" refers to the state and the uppercase superscript refers to the molecular framework. On the other hand, if the spin population is localized on the right, one has the B state.

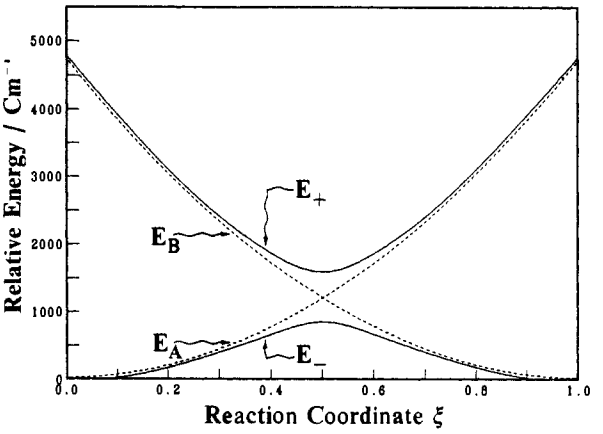

Figure 3. Diabatic (hashed curves) and adiabatic (solid curves) reaction profiles of molecule **1** at the 3-21G//3-21G level. The reaction coordinate ξ linearly combines Q_A and Q_B through $Q = \xi Q_B + (1 - \xi)Q_A$.

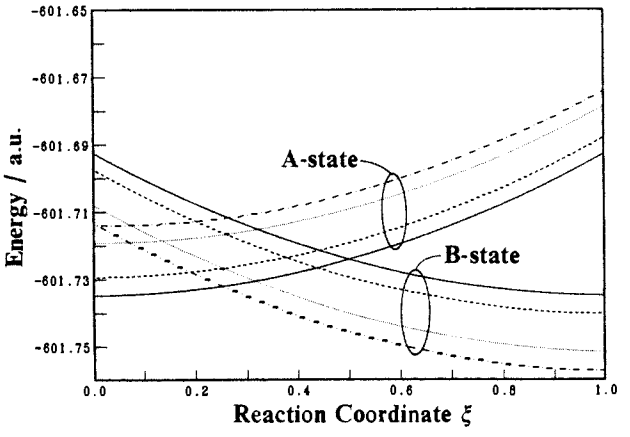

Figure 4. Electric field dependence of the diabatic reaction profile and the crossings of A state with B state at the STO-3G//STO-3G level. The electric field strengths are 0.000 (solid curves), 0.001 (dashed curves), 0.003 (dotted curves), and 0.004 (dash–dot curves) au.

In the absence of an external field (i.e., $F = 0$) the double-well potential in Figure 1 is symmetric, which means $E_A^A = E_B^B$ and $E_B^A = E_A^B$. In general, $E_A^A \neq E_B^A$ and $E_B^B \neq E_A^B$ unless we are dealing with the barrier-free case discussed in later sections. In addition, at the seam of the crossing, the energy of the A state is equal to that of the B state, i.e., $E_A^C = E_B^C$. Note that the B frame can be obtained from the A frame by a 180° rotation about the y axis (the axis that passes through the spiro carbon and is perpendicular to the PC plane) followed by a 90° rotation about the z axis shown in Figure 2.

Approximate Reaction Coordinate: Electric Field Effects. Having calculated the stable geometries Q_A and Q_B of the initial and final state, respectively, we want to know what pathway the reaction takes leading from Q_A to Q_B. This is the so-called "reaction coordinate", which is defined as the steepest descent pathway (in the many-dimensional nuclear coordinate space) passing through the global minimum point Q_C on the crossing seam surface.[34] Determination of the reaction coordinate in a system like ours with many nuclear degrees of freedom is a difficult task.[35] In the present case we use some intuition and define an ad hoc reaction coordinate.

We recall that molecule **1** consists of two rigid cyclic π-electron moieties (C and PC) connected to each other by again a rigid spirocycloalkane σ bridge. Therefore, it is reasonable to expect that any conformational change will cost a significant amount of energy for such an inflexible molecule. Hence, during the reaction the nuclear configuration changes slowly and smoothly from Q_A

(28) Dupuis, M.; Rys, J.; King, H. F. *J. Chem. Phys.* **1976**, *65*, 111. Dupuis, M.; Mougenot, P.; Watts, J. D.; Hurst, G. J. B.; Villar, H. O. In *Modern Techniques in Computational Chemistry*; Clementi, E., Ed.; MOTECC-89; ESCOM Science Publishers: Leiden, 1989.

(29) King, H. F.; Stanton, R. E.; Kim, H.; Wyatt, R. E.; Parr R. G. *J. Chem. Phys.* **1967**, *47*, 1936.

(30) Newton, M. D. *J. Phys. Chem.* **1988**, *92*, 3049.

(31) Ohta, K.; Morokuma, K. *J. Phys. Chem.* **1987**, *91*, 401.

(32) Boys, S. F. *Rev. Mod. Phys.* **1960**, *32*, 306. Foster, J. M.; Boys, S. F. *Ibid.* **1960**, *32*, 300. Boys, S. F. *Quantum Theory of Atoms, Molecules and the Solid State*; Löwdin, P.-O., Ed.; Academic Press: New York, 1966; p 253.

(33) Binckley, J. S.; Pople, J. A.; Hehre, W. J. *J. Am. Chem. Soc.* **1980**, *102*, 939.

(34) Kato, S.; Jaffe, R. L.; Komornicki, A.; Morokuma, K. *J. Chem. Phys.* **1983**, *78*, 4567.

(35) Determination of just Q_C without the whole reaction coordinate is quite possible. See: Koga, N.; Morokuma, K. *Chem. Phys. Lett.* **1985**, *119*, 371. Farazdel, A.; Dupuis, M., submitted for publication.

Table I. Computed Equilibrium Bond Lengths (in Angstroms) and Bond Angles (in Degrees) for the A State of the Molecular Cation 1 with C_{2v} Symmetry[a]

	cation		neutral
	3-21G	STO-3G	STO-3G
N_9-C_8	1.380	1.393	1.396
N_1-C_2	1.369	1.387	
C_8-C_7	1.358	1.351	1.349
C_2-C_3	1.430	1.448	
C_7-C_7	1.415	1.418	1.421
C_3-C_3	1.354	1.350	
C_7-C_6	1.501	1.510	1.512
C_3-C_4	1.500	1.513	
C_6-C_5	1.588	1.585	1.586
C_4-C_5	1.590	1.587	
$\angle C_8N_9C_8$	110.1	109.8	109.4
$\angle C_2N_1C_2$	109.7	109.8	
$\angle N_9C_8C_7$	106.8	106.5	106.7
$\angle N_1C_2C_3$	107.1	106.6	
$\angle C_7C_7C_6$	112.3	112.0	111.7
$\angle C_3C_3C_4$	113.3	113.0	
$\angle C_7C_6C_5$	104.1	104.5	105.0
$\angle C_3C_4C_5$	103.6	103.9	
$\angle C_6C_5C_6$	107.2	107.0	106.4
$\angle C_4C_5C_4$	106.1	106.0	

[a] Results for the neutral analogue of 1 with D_{2d} symmetry is also given for comparison. The numbering scheme of the atoms is given in Figure 2.

to Q_B going through Q_C. This is the rationale behind our choosing the reaction coordinate ξ such that Q_A and Q_B are mixed linearly:

$$Q = \xi Q_B + (1 - \xi)Q_A \qquad (10)$$

where Q is the nuclear configuration at any point on the assumed reaction path. In both Q_A and Q_B, the spiro carbon (C_5 in Figure 2) is defined as the origin of the coordinate system. In other words, during the ET reaction the spiro carbon remains stationary. The quantity ξ was varied from 0 (corresponding to the A frame) to 1 (corresponding to the B frame) in steps of 0.1. Then calculations were carried out for both A state and B state at zero-field strength and diabatic curves E_A and E_B were determined. An example of calculated reaction profiles at the 3-21G//3-21G level is illustrated in Figure 3. The adiabatic curves E_+ and E_- shown in Figure 3 were obtained by solving eq 1.

We varied the strength of the applied field, which is in the direction of the z axis shown in Figure 2. The resulting diabatic reaction profiles at the STO-3G//STO-3G level are shown in Figure 4. As expected, at zero-field strength, the two diabatic curves have identical shapes (symmetric double-well) and necessarily $\xi_C = {}^1/_2$ where $Q_C = Q(\xi = \xi_C)$. The effect of the electric field on the reaction profiles can be qualitatively understood in terms of the charge localization or dipole moment of the molecule. For the A state, the positive charge is localized on the left, i.e., the dipole moment[36] vector is in the $-z$ direction. Hence, increasing the field along the $+z$ direction in turn increases the total energy of the A state. Conversely, the dipole moment of the B state is in the $+z$ direction and increasing the field strength lowers the total energy. Consequently, as the field strength increases, the crossing occurs earlier on the ξ axis (i.e., ξ_C decreases; see also eq 28) and the diabatic activation energy (see next section) also decreases.

There is an interesting aspect to the variation of ξ_C versus the field strength F. The electric field at which $\xi_C = 0$ (i.e., $Q_C = Q_A$) is designated by F_{thresh}. At this threshold field we have the barrier-free case and the diabatic activation energy vanishes (see Figure 7 and later sections). At fields below F_{thresh}, we have what

(36) All dipole moment values referred in this work are with respect to the center of mass of the molecule.

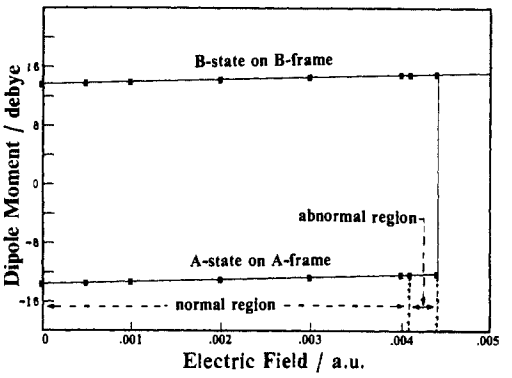

Figure 5. Variation of the dipole moment of molecule 1 versus the external electric field strength. For definitions of the different regions refer to the text.

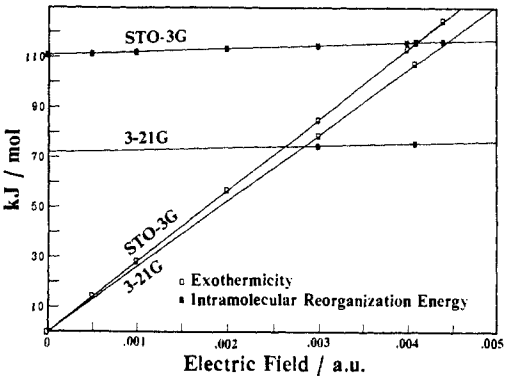

Figure 6. Electric field dependence of intramolecular reorganization energy and exothermicity. The observed trends are rationalized in the text by using a simple model.

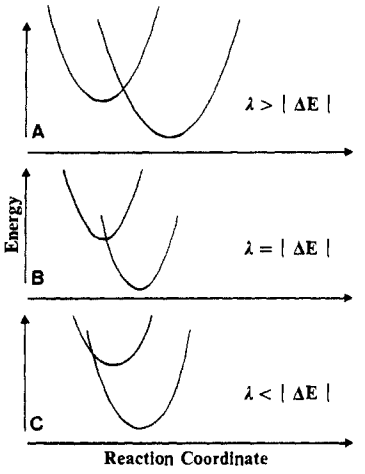

Figure 7. Schematic diabatic potential energy surfaces for (A) normal region $\lambda > |\Delta E|$, (B) barrier-free case $\lambda = |\Delta E|$, and (C) inverted region $\lambda < |\Delta E|$.

is usually referred to as the "normal"[12] region: normal in a sense that for the ET process an Arrhenius-type equation (eq 4) is still suitable and the activation energy is a positive quantity. At fields higher than F_{thresh} the system is in the "abnormal" region[12] (see Figures 5–7). We plot ξ_C versus F and extrapolate to $\xi_C = 0$ and find F_{thresh}. The results are 0.004 09 au at the STO-3G and 0.002 86 au at the 3-21G level. One word of caution is in order here. In addition to the type of basis set used, Q_A, Q_B, and consequently the reaction coordinate ξ depend on the applied electric field strength. This dependence was neglected in our calculations reported here (unless otherwise stated) since the applied field is a weak one. In any event, it was observed that beyond F_{thresh} one can get both A-state and B-state solutions until a second threshold field F_{limit} (at STO-3G, F_{limit} had the value of 0.0044) is reached, beyond which we were not successful in

forcing the calculation into the A state, i.e., the two wells had collapsed into a single well.

Energetics: Electric Field and Basis Set Effects. ET reactions like any other reaction are characterized by energy changes. We calculated the intramolecular reorganization energy (energy associated with changes in nuclear configuration of the molecule upon the transfer of electron) $\lambda = E_B^A - E_B^B$, the exothermicity $|\Delta E| = E_A^A - E_B^B$, the diabatic activation energy $E_d = E_A^C - E_A^A$ and the adiabatic activation energy $E_a = E_d - V_{AB}$ (Figure 1). In particular, we examined how these quantities vary with the electric field strength and their sensitivity to the choice of basis set. At zero field, we obtained E_d = 2236, 1100, and 1081 cm^{-1} using STO-3G, 3-21G, and then 3-21G augmented by three diffuse SP shells (exponents of 0.1, 0.05, and 0.01), but only for the spiro carbon (hereafter we designate the latter basis set as 3-21Gddd). As will be noted later, V_{AB} is much less sensitive to the choice of basis set than E_d. Our calculated values for the adiabatic activation energies are 1948, 733, and 717 cm^{-1} for the above-mentioned basis sets, respectively. The Q_A and Q_B used for the above results were all at the STO-3G level. But when we used Q_A and Q_B at the 3-21G level, the result was E_d = 1181 cm^{-1} and E_a = 821 cm^{-1}, using the 3-21G basis set. We see that the general trend observed for the STO-3G case is still valid. Figure 6 shows the results for intramolecular reorganization energy and exothermicity with the STO-3G and 3-21G basis sets at different electric field strengths. It is interesting to note that although exothermicity increases linearly with the field strength, the intramolecular reorganization energy stays nearly unchanged. This and some other behaviors are explained by a model described in the next section.

A Simple Model for Electric Field Dependence of the Diabatic Reaction Profiles. Here we seek simple analytic expressions that accurately represent the variation of total energy of the molecule with respect to the reaction coordinate ξ and applied field strength F. Then we derive expressions for the ET properties of molecule **1** in terms of ξ and F. A knowledge of this type is useful if we are to manipulate the ET characteristics of **1** by structural engineering and chemical modifications. In addition, we rationalize the trends observed in the ET properties reported in this work in terms of a few calculated parameters.

Inspection of Figure 4 reveals several informative features. As can be seen, for a given nuclear configuration or equivalently for a given ξ, the shift in energy is proportional to the electric field strength.[37] This is expected due to the smallness of the applied field, which is in the range of 0.0–0.005 au of field strength. As usual for such a weak field, the total Hamiltonian of the molecule, $\mathcal{H}$ (not to be confused with the electronic Hamiltonian H referred to earlier), can be written as[6]

$$\mathcal{H} = \mathcal{H}^{(0)} - \mu_z F_z - \dots \quad (11)$$

since the electric field in our case is applied in the z direction, i.e., $F_x = F_y = 0$. Here $\mathcal{H}^{(0)}$ is the total Hamiltonian for the free molecule and μ_z is the z component of the usual dipole moment operator. If the molecule is in the quantum state Ψ, its energy for a fixed position and orientation is given by

$$E(\xi, F_z) = \langle\Psi|\mathcal{H}|\Phi\rangle = E(\xi, 0) - \mu_z(\xi, 0)F_z - \tfrac{1}{2}\alpha_{zz}(\xi, 0)F_z^2 - \dots \quad (12)$$

where $\mu_z(\xi, 0) = \langle\Psi^{(0)}|\mu_z|\Psi^{(0)}\rangle$ is the permanent dipole moment of the molecule, $\Psi^{(0)}$ is the unperturbed wave function [i.e., $\mathcal{H}^{(0)}\Psi^{(0)} = E(\xi, 0)\,\Psi^{(0)}$] and α_{zz} is the appropriate component of the molecular polarizability tensor. Since the energy shift is proportional to F, taking only the first two terms in eq 12 is sufficient for our simple model. Therefore, the total energy of the A state and that of the B state as a function of F can be written as

$$E_i(\xi, F) = E_i(\xi, 0) - \mu_i(\xi, 0)F \quad i = \text{A, B} \quad F \geq 0 \quad (13)$$

where for the sake of convenience, the subscript "z" is dropped from μ and F. Recall that for our choice of coordinate system, $\mu_A < 0$ but $\mu_B > 0$. In addition, due to the symmetry relationship referred to earlier, between the A frame and the B frame,

$$\mu_A(\xi, 0) = -\mu_B(1 - \xi, 0) \quad (14)$$

We are now interested in describing the dependence of $E_i(\xi, 0)$ on ξ. The actual numerical data of Figure 4 show that, at a given field strength F, the total energy varies harmonically according to Hooke's law. This is not surprising since variation of ξ from 0 to 1 amounts to a small change in the nuclear configuration (see Table I and compare the dimensions of the two sides of the molecule **1**). This means the molecule remains very close to the minimum of the energy during the ET reaction, and hence Hooke's law. Therefore, the energy of the A state can be represented by

$$E_A(\xi, 0) = -a + b\xi^2 \quad (15)$$

and that of the B state by

$$E_B(\xi, 0) = -a + b(1 - \xi)^2 \quad (16)$$

since the minimum of $E_A(\xi, 0)$ is at $\xi = 0$ while for $E_B(\xi, 0)$ at $\xi = 1$. Note that in eqs 15 and 16

$$a = -E_A^A = -E_B^B > 0;\ b = E_A^B + a = E_B^A + a > 0 \quad (17)$$

All energy quantities in eq 17 are at $F = 0$. For example $E_A^A = E_A(0, 0)$, $E_A^B = E_A(1, 0)$, etc. The parameter b can also be identified as the intramolecular reorganization energy (see Figure 1).

Similarly we want to express the dependence of the permanent dipole moment of the free molecule on ξ. Again from Figure 4 we see that for a given state (A state or B state), the diabatic reaction profiles are approximately parallel to each other for different values of F. This implies that the dipole moment is but weakly dependent on ξ. Closer inspection of the numerical data, however, shows that at a given F, the dipole moment varies linearly versus ξ with a small slope, i.e.,

$$\mu_A(\xi, 0) = -\alpha + \beta\xi \quad (18)$$

and according to eq 14

$$\mu_B(\xi, 0) = +\alpha - \beta(1 - \xi) \quad (19)$$

Here

$$\alpha = -\mu_A^A = \mu_B^B > 0;\ \beta = \mu_A^B + \alpha = -\mu_B^A + \alpha > 0 \quad (20)$$

where all dipole moments are with respect to the center of mass of the molecule and at $F = 0$. For example $\mu_A^A = \mu_A(0, 0)$, $\mu_A^B = \mu_A(1, 0)$, etc. The second inequality in eq 20 may not be true in general but its validity is supported by numerical data in our case.

From eqs 13, 15, 16, 18, and 19 we obtain

$$E_A(\xi, F) = b\xi^2 - \beta F\xi - a + \alpha F \quad (21)$$

and

$$E_B(\xi, F) = b\xi^2 - (\beta F + 2b)\xi - a + b - (\alpha - \beta)F \quad (22)$$

Consequently, according to our model, E_A and E_B as a function of ξ are two parabolas with identical curvature b, which is independent of the field strength F. The minimum of E_A is at

$$\xi_A = \beta F/2b \quad (23)$$

and that of E_B at

$$\xi_B = 1 + \beta F/2b \quad (24)$$

In words, as F increases from 0, both minima are shifted by the same amount $\beta F/2b$. This shift is negligible in our case because it is smaller than the mesh on the ξ axis. For example at the 3-21G level $b = 2.7409 \times 10^{-2}$ au = 71.963 kJ/mol, α = 4.902, and β = 0.219 au of dipole moment. Hence, the maximum shift (i.e., at F = 0.005 au) is only 0.02 while our mesh is 0.1.

This simple model can predict the observed calculated behaviors both qualitatively and quantitatively to a large extent. For instance

(37) In addition to visual inspection, the actual numerical data show the same.

for the intramolecular reorganization energy we have (using eqs 13 and 20)

$$\lambda_{appr}(F) = E_B(0, F) - E_B(1, F) = b + \beta F \quad (25)$$

in complete agreement with Figure 6. The subscript "appr" emphasizes that the shift of minima given by eqs 23 and 24 is neglected. In fact, if the shift is included, we get

$$\lambda(F) = E_B(\xi_A, F) - E_B(\xi_B, F) = b \quad (26)$$

which is independent of F. For the exothermicity we have

$$|\Delta E(F)| = E_A(\xi_A, F) - E_B(\xi_B, F) = E_A(0, F) - E_B(1, F) = 2\alpha F \quad (27)$$

Agin in agreement with Figure 6 at both STO-3G and 3-21G levels.

Similarly we can describe the variation of ξ_C, the reaction coordinate parameter at the crossing point, with the electric field strength. From eqs 13, 15, 16, 18, and 19 and the condition $E_A(\xi_C, F) = E_B(\xi_C, F)$ we obtain

$$\xi_C(F) = \frac{1}{2} - \frac{2\alpha - \beta}{2b} F \quad (28)$$

in agreement with Figure 4. The numerical results of eq 28 are practically the same as the ones obtained from crossing the actual computed diabatic surfaces. The quantity $2\alpha - \beta$ in eq 28 can be identified (see eq 20) as $\mu_B^B + \mu_B^A$, i.e., dipole moment of the B state on B frame plus that of the B state on A frame.

Barrier-Free Case: Threshold Field. Intuitively, as the electric field strength increases, the energy of the A state increases while that of the B state decreases and hence the diabatic activation energy E_d also decreases (see Figure 4). The field strength at which $E_d = 0$ is designated as F_{thresh}. In this case, which is also called "barrier-free", the minimum of the left well in the double-well potential coincides with the potential curve of the right well (Figure 7B), i.e., $\lambda = |\Delta E|$. Below F_{thresh}, we have the "normal" region[11,12] (Figure 7A) where Q_C is between Q_A and Q_B and hence $\lambda > |\Delta E|$. Otherwise, (i.e., $\lambda < |\Delta E|$), Q_C would be outside the range of Q_A and Q_B and it is referred to as the "inverted region" (Figure 7C).[12] The value of F_{thresh} can be estimated by using eqs 25 and 27 along with the condition $\lambda(F) = |\Delta E(F)|$

$$F_{thresh,appr} = b/(2\alpha - \beta) \quad (29)$$

or by using eqs 26 and 27

$$F_{thresh} = b/2\alpha \quad (30)$$

The validity of eq 29 was checked by computing $F_{thresh,appr}$ from it and comparing it to the value from extrapolation. The numerical results were virtually identical ($F_{thresh,appr} = 0.00286$ au at the 3-21G level). Equations 29 and 30 can also be derived from eq 28 realizing that $\xi_C(F = F_{thresh,appr}) = 0$ and $\xi_C(F = F_{thresh}) = \beta F_{thresh}/2b$. For the molecule to be used as a molecular device, practical considerations demand F_{thresh} not to exceed 5×10^6 V/cm = 0.001 au. This may be achieved by minor structural or chemical modifications of the molecule.

V_{AB} Term: Electric Field and Basis Set Effects. The electron-transfer matrix V_{AB} values reported in this work were calculated explicitly from the nonorthogonal charge-localized UHF states Ψ_A and Ψ_B according to the formulas given in the Appendix and eq 2.[38] It was found that V_{AB} is insensitive to variations in external field strength. For example, with an STO-3G basis set, V_{AB} = 287.622, 287.405, and 284.420 cm^{-1} at field strengths of 0 ($\xi_C = 0.5$), 0.001 ($\xi_C = 0.367$), and 0.00409 ($\xi_C = 0$; i.e., A frame) au. At first, one might suspect that STO-3G is not flexible enough to show the change in V_{AB} due to change in the field strength. But when the 3-21G basis set was used, the results were V_{AB} = 366.760, 364.370, and 370.277 cm^{-1} at field strengths of 0 ($\xi_C = 0.5$), 0.002833 ($\xi_C = 0$), and 0.00409 (at A frame). One sees that although the value of V_{AB} has increased when the more flexible basis set is used, its variations with respect to the external field are still negligible. The calculation at zero field was repeated with the more extensive 3-21Gddd basis set. The result was V_{AB} = 363.6 cm^{-1}, i.e., a change of less than 1% compared to the 3-21G results.

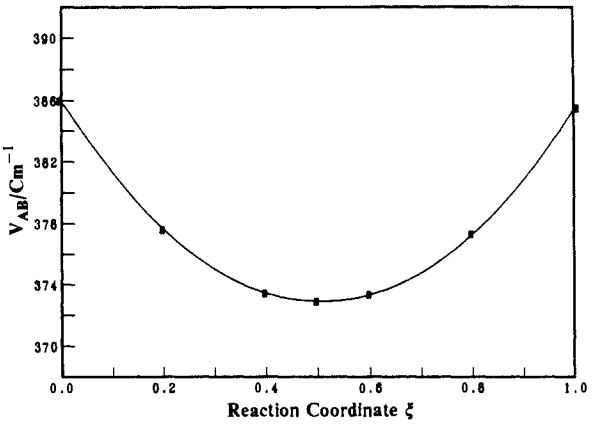

Figure 8. Variation of V_{AB} with respect to the reaction coordinate at the 3-21G//3-21G level indicating the validity of the Condon approximation for the title molecule.

Since the planes of the C and PC π-electron moieties are prependicular to each other, one might expect the V_{AB} values to be perhaps smaller than the one reported here. This can be rationalized in a one-electron picture as follows. According to our results, the electron jumps from a left-localized MO with a_2 symmetry (C_{2v} point group) to a right-localized MO also with a_2 symmetry (these orbitals are made up of the C=C π bonds of the pyrrole groups). The tails of these localized MOs with the same symmetry are responsible for the nonzero value of the overlap S_{AB}, and consequently of H_{AB} (in the spirit of the extended Hückel model in which it is assumed that $H_{AB} \propto S_{AB}$) and therefore of V_{AB} (see eq 2). For an insightful analysis of V_{AB} in terms of various orbital concepts, see ref 30.

V_{AB} Term: Nuclear Configuration Effect. As we discussed earlier in the quantum mechanical description of ET (eqs 7–9), usually it is assumed that V_{AB} given by eq 2 (not to be confused with $^1/_2\Delta$, half of the separation between E_+ and E_-; see Figure 3) is a weak function of the nuclear coordinates. Hence, the numerical value of V_{AB} remains roughtly constant as long as the nuclear coordinates correspond to the vicinity of Q_C. In fact, this assumption, which is commonly referred to as the Condon approximation,[7] enables us to arrive at eq 8 from eq 7. To evaluate the validity of this approximation for our molecule, we calculated V_{AB} according to eq 2 at different points on the reaction coordinate. The results are shown in Figure 8. We see that the variation of V_{AB} with respect to nuclear configuration along the reaction coordinate is rather small, at most about 3%. So the Condon approximation is quite valid for molecule **1**.

Activation Energies and Electron-Transfer Rate: Electric Field Effect. We are now in a position to see how the electron-transfer rate changes by increasing the applied field strength F. According to Marcus' model (eq 3) the relevant quantities are κ and $\Delta H^{\ddagger}$. The latter quantity can be approximated by the diabatic activation energy E_d. According to the Landau–Zener formula,[26] at a given temperature, κ depends on V_{AB} and the slopes of the diabatic potential curves A and B at the crossing seam. We mentioned earlier that none of these quantities change significantly with the electric field strength. Hence, the main contribution to the change in ET rate comes from E_d. We can derive an expression for E_d within the framework of our model, using eqs 13, 15, 18, and 28.

$$E_d(F) = E_A(\xi_C, F) - E_A(\xi_A, F) = (1/4b)(b - 2\alpha F)^2 \quad (31)$$

Note that $E_d(0) = b/4$ as expected for any symmetric harmonic

(38) As a consistency check, we also evaluated some of our V_{AB} values using an alternative formulation, which is based on delocalized solutions rather than the localized ones that we have used in this report. See: Newton, M. D. *Adv. Chem. Ser.* **1982**, *No. 198*, 255.

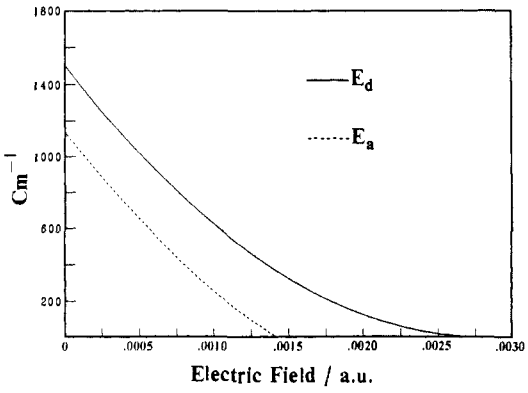

Figure 9. Variation of the diabatic activation energy E_d and the adiabatic activation energy E_a with respect to the external electric field strength at the 3-21G//3-21G level.

double-well potential. We also see that E_d has its maximum value at zero field and then monotonically goes to zero at the field strength of $F_{thresh} = b/2\alpha$, as expected from eq 30. Recall that the adiabatic activation energy E_a can be obtained from $E_a = E_d - V_{AB}$, where V_{AB} is effectively independent of the field strength F. Figure 9 shows both E_d and E_a versus F at the 3-21G//3-21G level.

At the 3-21G level, $\alpha = 4.902$ au and $b = 0.027\,409$ au; hence, $F_{thresh} = 2.796 \times 10^{-3}$. In the normal region (i.e., $F < F_{thresh}$), Marcus' model is applicable and the electron-transfer rate $k_{et}(F)$ as a function of F increases exponentially. For instance, at room temperature ($k_BT = 9.50 \times 10^{-4}$ au) we have[23]

$$k_{et}(0.0):k_{et}(0.001):k_{et}(2.796 \times 10^{-3}) \simeq 1:69:1357$$

Through-Bond and Through-Space ET. In order for a molecule to be used as a molecular electronic device, it is desirable to be able to fine tune its electron-transfer characteristics (V_{AB}, F_{thresh}, ...) by chemical and structural modifications of the σ bridge. This is possible if the chemical bonds that make up the σ bridge are mostly responsible for the transfer of electrons. In this case, which is usually referred to as the through-bond ET, the transfer of electrons between C and PC units, proceeds by way of an intermediate electronic state that uses wave functions localized on the σ bridge. In contrast, the so-called through-space ET is the result of the direct spatial overlap of the C and PC wave functions while the σ bridge is used only to bring the two units together. To estimate the through-space contribution, we calculated V_{AB} at zero field for a supermolecule consisting of a pyrrole and a pyrrole cation located at the same distance and angle (90°) as the corresponding structure at the seam of crossing for molecule **1**. Here we augmented the basis set of all carbons by the previously mentioned three SP shells. Using such an extensive basis set assures us of the flexibility needed for the two fragments to overlap through space. The result was 31.3 cm^{-1}, i.e., through-space contribution to V_{AB} is less than 9% of the total (V_{AB} = 363.6 cm^{-1})—a desirable characteristic for **1** as a molecular device.

Summary and Conclusions

The LCAO–MO SCF ab initio electronic structure method was used to study the intramolecular electron-transfer characteristics of the title molecular cation (**1**)—a molecular device model molecule. In particular, the effects of an external electric field on potential energy surfaces, energetics, and electron-transfer matrix element were considered. Our study establishes that **1** is a double-well-potential molecule with a significant barrier against the transfer of electrons from one end of the molecule to the other end. The barrier is sufficiently high so the stored bit of information is not inadvertently lost. This barrier height decreases (i.e., electron-transfer rate increases) rapidly as the external field strength is increased (see eq 31). The field strength at which the barrier height vanishes is about 0.0028 au $\simeq 1.4 \times 10^7$ V/cm.

While the barrier height is sensitive to the applied field strength, the electron-tranfer matrix element is not. We also find that exothermicity is proportional to the applied field but the intramolecular reorganization energy remains constant. A simple model was presented that explains the above observations. Finally, it was shown that the electron transfer for **1** is dominated by a through-bond rather than a through-space mechanism—a feature that is desired in molecular devices.

Acknowledgment. We thank Professor Mark A. Ratner for a critical reading of the manuscript and making many helpful suggestions.

Appendix: Calculation of V_{AB}

Let Ψ_A and Ψ_B be the two nonorthogonal diabatic UHF wave functions representing left- and right-localized spin densities. The more strongly these wave functions are localized the more suitable they would be for our two-state model. Being UHF wave functions, each constituent molecular spin orbital of Ψ_A, $\mathbf{a} = (a_1, a_2, ..., a_N)$, has a nonzero overlap with each and every spin orbital of Ψ_B, $\mathbf{b} = (b_1, b_2, ..., b_N)$, with the same spin, i.e., the overlap matrix **D**

$$\mathbf{D} = \int \mathbf{b}^\dagger \mathbf{a}\, d\tau \tag{A-1}$$

is not necessarily diagonal. As a result, the expressions for direct calculation of matrix elements S_{AB} and H_{AB}, which are needed for the computation of V_{AB} via eq 2, become cumbersome. In order to simplify the evaluation, we use the method of the *corresponding orbital transformation*.[29] In this procedure, each set of spin orbitals **a** and **b** are linearly transformed

$$\hat{\mathbf{a}} = \mathbf{a}\mathbf{V} \tag{A-2}$$

$$\hat{\mathbf{b}} = \mathbf{b}\mathbf{U} \tag{A-3}$$

in such a way that the overlap matrix between the two new sets

$$\hat{\mathbf{d}} = \int \hat{\mathbf{b}}^\dagger \hat{\mathbf{a}}\, d\tau = \mathbf{U}^\dagger \mathbf{D} \mathbf{V} \tag{A-4}$$

is diagonal. In our case **D** is a real matrix, hence eq A-4 is the singular value decomposition of **D** with diagonal elements of the diagonal matrix $\hat{\mathbf{d}}$ being the singular values. **U** and **V** are real unitary matrices. In this Appendix we develop expressions for the evaluation of S_{AB} and H_{AB} in terms of eigenvectors and overlap matrix of an LCAO–MO calculation.

Let us expand the molecular spin orbitals **a** and **b** in terms of a common basis set $\chi = (\chi_1, \chi_2, ..., \chi_M)$, i.e.,

$$\mathbf{a} = \chi\mathbf{A} \tag{A-5}$$

and

$$\mathbf{b} = \chi\mathbf{B} \tag{A-6}$$

Now, by use of eqs A-5, A-6, A-2, and A-3, the one-electron contribution to H_{AB} (eq 22 of ref 29) becomes

$$\begin{aligned}\Omega_{AB}^{(1)} &= (\det \mathbf{U})(\det \mathbf{V}^\dagger)\sum_i^N \langle \hat{b}_i|\omega|\hat{a}_i\rangle T_{ii} \\ &= (\det \mathbf{U})(\det \mathbf{V}^\dagger)\sum_i^N \sum_{\mu\nu}^M \hat{A}_{\mu i} T_{ii} \hat{B}_{i\nu}^\dagger \omega_{\mu\nu} \\ &= (\det \mathbf{U})(\det \mathbf{V}^\dagger)\sum_{\mu\nu}^M P_{\mu\nu}\omega_{\mu\nu}\end{aligned} \tag{A-7}$$

where $T_{ii} = \prod_{j\neq i}^N \hat{d}_{jj}$, $\omega_{\mu\nu} = \langle \chi_\mu|\omega|\chi_\nu\rangle$ with ω denoting the one-electron operator and we have introduced three new matrices $\hat{\mathbf{A}} = \mathbf{AV}$, $\hat{\mathbf{B}} = \mathbf{BU}$, and $\mathbf{P} = \hat{\mathbf{A}}\mathbf{T}\hat{\mathbf{B}}^\dagger$. Note that **P** can be looked upon as a "generalized" density matrix in a sense that when there is no transformation (i.e., $\mathbf{U} = \mathbf{V} = \mathbf{I}$), **P** will reduce to the standard density matrix.

Similarly, the two-electron contribution (eq 23 of ref 29) is

$$\begin{aligned}\Omega_{AB}^{(2)} &= \\ &(\det \mathbf{U})(\det \mathbf{V}^\dagger)(\mathrm{prod})^{-1}\sum_{i<j}^N T_{ii}T_{jj}\, \langle \hat{b}_i\hat{b}_j|\omega(1,2)(1 - P_{12})|\hat{a}_i\hat{a}_j\rangle \\ &= \tfrac{1}{2}(\det \mathbf{U})(\det \mathbf{V}^\dagger)(\mathrm{prod})^{-1}\sum_{ij}^N \sum_{\mu\nu\lambda\sigma}^M T_{ii}T_{jj}\hat{A}_{\lambda i}\hat{A}_{\sigma j}\hat{B}_{i\mu}{}^\dagger \hat{B}_{j\nu}{}^\dagger \times \\ &\qquad \langle \chi_\mu\chi_\nu|\omega(1,2)(1 - P_{12})|\chi_\lambda\chi_\sigma\rangle \\ &= \tfrac{1}{2}(\det \mathbf{U})(\det \mathbf{V}^\dagger)(\mathrm{prod})^{-1}\sum_{\mu\nu\lambda\sigma}^M P_{\lambda\mu}P_{\sigma\nu}\langle \chi_\mu\chi_\nu|\omega(1,2) \times \\ &\qquad (1 - P_{12})|\chi_\lambda\chi_\sigma\rangle\end{aligned}$$

where prod = $\prod_{k=1}^{N}\hat{d}_{kk}$, $\omega(1,2)$ denotes the Coulombic interaction between electrons 1 and 2; and P_{12} is the usual permutation operator. If we adopt the standard chemist's notation for two-electron integrals, the last equation may be written as

$$\Omega_{AB}^{(2)} = \tfrac{1}{2}(\det \mathbf{U})(\det \mathbf{V}^{\dagger})(\mathrm{prod})^{-1}\sum_{\mu\nu\lambda\sigma}^{M} P_{\mu\nu}P_{\lambda\sigma}\{\langle\mu\nu|\lambda\sigma\rangle - \langle\mu\sigma|\lambda\nu\rangle\} \quad \text{(A-8)}$$

Here $\langle\mu\nu|\lambda\sigma\rangle = \langle\chi_\mu\chi_\lambda|\omega(1,2)|\chi_\nu\chi_\sigma\rangle$. Now let us specialize the above formulas for our particular case in which the molecular orbitals are either α spin or β spin. In this case the overlap matrix **D** is block diagonal and so are **V**, **U**, $\hat{\mathbf{d}}$, **A**, **B**, and **P**. As a result we have (from eq A-7)

$$\Omega_{AB}^{(1)} = (\det \mathbf{U})(\det \mathbf{V}^{\dagger})\{\sum_{\mu\nu}^{M} P_{\mu\nu}^{\alpha}\omega_{\mu\nu} + \sum_{\mu\nu}^{M} P_{\mu\nu}^{\beta}\omega_{\mu\nu}\}$$

or

$$\Omega_{AB}^{(1)} = (\det \mathbf{U})(\det \mathbf{V}^{\dagger})\sum_{\mu\nu}^{M} P_{\mu\nu}^{t}\omega_{\mu\nu} \quad \text{(A-9)}$$

where $\mathbf{P}^t = \mathbf{P}^\alpha + \mathbf{P}^\beta$. It is also assumed that the trivial spin integration in $\omega_{\mu\nu}$ is already performed.

Similarly, from eq A-8 we get

$$\Omega_{AB}^{(2)} = \tfrac{1}{2}(\det \mathbf{U})(\det \mathbf{V}^{\dagger}) \times (\mathrm{prod})^{-1}\{\sum_{\mu\nu\lambda\sigma}^{M} P_{\mu\nu}^{\alpha}P_{\lambda\sigma}^{\alpha}[(\mu\nu|\lambda\sigma) - (\mu\sigma|\lambda\nu)] + \sum_{\mu\nu\lambda\sigma}^{M} P_{\mu\nu}^{\alpha}P_{\lambda\sigma}^{\beta}(\mu\nu|\lambda\sigma) + \sum_{\mu\nu\lambda\sigma}^{M} P_{\mu\nu}^{\beta}P_{\lambda\sigma}^{\alpha}(\mu\nu|\lambda\sigma) + \sum_{\mu\nu\lambda\sigma}^{M} P_{\mu\nu}^{\beta}P_{\lambda\sigma}^{\beta}[(\mu\nu|\lambda\sigma) - (\mu\sigma|\lambda\nu)]\}$$

or after some simple manipulations we get

$$\Omega_{AB}^{(2)} = \tfrac{1}{2}(\det \mathbf{U})(\det \mathbf{V}^{\dagger}) \times (\mathrm{prod})^{-1}\sum_{\mu\nu\lambda\sigma}^{M}[P_{\mu\nu}^{t}P_{\lambda\sigma}^{t} - P_{\mu\nu}^{\alpha}P_{\lambda\sigma}^{\alpha} - P_{\mu\nu}^{\beta}P_{\lambda\sigma}^{\beta}](\mu\nu|\lambda\sigma) \quad \text{(A-10)}$$

Here $(\mu\nu|\lambda\sigma)$ is similar to $\langle\mu\nu|\lambda\sigma\rangle$ except in the former the spin integration is already done. Note that eqs A-9 and A-10 bear a formal resemblance to that of standard one-electron and two-electron sums in LCAO-MO methods.

Our program module linked to the HONDO package consists of the following steps:

1. Carry out steps 2-5 below for both α- and β-occupied molecular orbitals.
2. Calculate the overlap matrix **D** from $\mathbf{D} = \mathbf{B}^{\dagger}\mathbf{S}\mathbf{A}$, where **A** and **B** are the eigenvectors of the diabatic states and **S** is the overlap matrix over atomic orbitals. The latter three matrices are part of standard output in LCAO-MO programs.
3. Perform the corresponding orbital transformation by computing the singular value decomposition of the real matrix **D** as $\mathbf{D} = \mathbf{U}\hat{\mathbf{d}}\mathbf{V}^{\dagger}$ and determine **U**, **V**, and the diagonal matrix $\hat{\mathbf{d}}$.
4. As an internal check, compute det **U** and det **V**. The absolute value of both quantities should be unity since **U** and **V** are unitary matrices.
5. Form matrices $\hat{\mathbf{A}}$ and $\hat{\mathbf{B}}$ as well as the diagonal matrix **T**, using $\hat{\mathbf{A}} = \mathbf{A}\mathbf{V}$, $\hat{\mathbf{B}} = \mathbf{B}\mathbf{U}$, and $T_{ii} = \prod_{j\neq i}^{N}\hat{d}_{jj}$. Then compute the generalized density matrix **P** by $\mathbf{P} = \hat{\mathbf{A}}\mathbf{T}\hat{\mathbf{B}}^{\dagger}$.
6. Compute S_{AB} from (eq 21 of ref 29)

$$S_{AB} = (\det \mathbf{U})(\det \mathbf{V}^{\dagger})(\mathrm{prod}) \quad \text{(A-11)}$$

7. Compute $\Omega_{AB}^{(1)}$ and $\Omega_{AB}^{(2)}$ by using eqs A-9 and A-10, respectively. Then compute H_{AB} by $H_{AB} = \Omega_{AB}^{(1)} + \Omega_{AB}^{(2)}$ and finally V_{AB} by using eq 2.

Dynamics of Ferrocene in a Thiourea Inclusion Matrix

Michael D. Lowery,[1] Richard J. Wittebort,*[2] Michio Sorai,[3] and David N. Hendrickson*[4]

Contribution from the Department of Chemistry, D-006, University of California at San Diego, La Jolla, California 92093-0506, Department of Chemistry, University of Louisville, Louisville, Kentucky 40292, School of Chemical Sciences, University of Illinois, Urbana, Illinois 61801, and Chemical Thermodynamics Laboratory, Faculty of Science, Osaka University, Toyonaka, Osaka 560, Japan. *Received May 30, 1989*

Abstract: ^{57}Fe Mössbauer and solid-state ^{2}H NMR spectroscopy are used to investigate the orientation and onset of motion of $Fe(C_5D_5)_2$ in the channels of the thiourea inclusion compound. ^{2}H NMR spectra obtained by rotating a single crystal of $Fe(C_5D_5)_2{\cdot}3(NH_2)_2CS$ about two orthogonal axes have been simulated and indicate that there are six different static ferrocene orientations at 140 K. At 140 K ~55% of the ferrocenes are located in three positions related by the crystallographic C_3 axis, where the ferrocene molecular axis is perpendicular to the channel axis of the thiourea host. The other three static ferrocene positions, which are interrelated by the C_3 axis, are located with the ferrocene molecular axis ~17° off the C_3 axis. In each of the perpendicular and parallel sites there is a distribution of ferrocene sites due to static disorder. Abruptly at the 160 K phase transition the perpendicular ferrocenes start jumping between the three perpendicular sites and the others start jumping between the three essentially parallel sites. Simulations of the Mössbauer spectra show that in the 160-225 K range the rate of interconversion of ferrocenes between perpendicular and parallel orientations is slower than ~10^5 s^{-1}. The Mössbauer spectrum changes from two doublets in the 160-220 K region to become one doublet and then a single Lorentzian peak in the 220-300 K range. Spectra for a single crystal show that the ^{2}H NMR spectrum collapses to a single doublet with a splitting of only 4.0 kHz with the field along the C_3 axis. A model is proposed that accounts not only for the spectroscopic observables but also for the heat capacity results, which show an entropy gain of $\Delta S \cong R \ln 4$ at the 160 K transition and little entropy gain in the 180-300 K range where the Mössbauer and ^{2}H NMR spectra change.

Since the accidental discovery by Bengen and Schlenk[5] that urea forms an inclusion compound with octal alcohol, urea and thiourea inclusion compounds have received considerable attention and are still the focus of active interest.[6] For example, Tam et

(1) University of Illinois.

(2) University of Louisville.

0002-7863/90/1512-4214$02.50/0